Chemical Papers (2021) 75:1555–1566
https://doi.org/10.1007/s11696-020-01388-8

ORIGINAL PAPER

Photocatalytic and fluorescent chemical sensing applications of La-doped ZnO nanoparticles

Manoj Kumar[1] · Kuldeep Negi[1] · Ahmad Umar[2,3] · M. S. Chauhan[1]

Received: 12 June 2020 / Accepted: 8 October 2020 / Published online: 13 November 2020
© Institute of Chemistry, Slovak Academy of Sciences 2020

Abstract

Herein, we report the facile solution phase precipitation synthesis of ZnO nanoparticles doped with various concentrations, i.e. 1, 5 and 10 mol% of lanthanum (La). The synthesized nanoparticles were characterized in detail by several techniques which confirmed the high-density growth and well-crystalline nature of La-doped ZnO nanoparticles. The XRD results revealed the successful incorporation of 1 mol% La ions in the hexagonal wurtzite structure of ZnO; however, small XRD peaks of La_2O_3 were detected in 5 and 10 mol% La-doped samples. All the La-doped nanoparticles were found to be UV responsive. For the application prospective, all the synthesized nanoparticles were used as photocatalyst for the photocatalytic degradation of three toxic dyes, i.e. methyl orange (MO), Rhodamine B (Rh B) dyes and picric acid (PA). By detailed photocatalytic investigations, interestingly, 1 mol% La-doped ZnO was found to be most efficient photocatalyst towards the degradation of all three organic dyes. Further, the synthesized nanoparticles were also used as fluorescent probe for the fluorescence sensing of picric acid (PA). Remarkably, the 1 mol% nanoparticles exhibited highest sensitivity, i.e. lowest limit of detection (LOD) value (1.05 μM L^{-1}) towards PA compared to 5 and 10 mol% (1.38 μM L^{-1}) La-doped ZnO nanoparticles.

Keywords La-doped ZnO nanoparticles · Photocatalysis · Fluorescent sensor

Introduction

Nanostructured zinc oxide (ZnO) is a promising semiconductor material because of its intriguing features, such as bio-compatibility, cost-effectiveness, large exciton binding energy (~ 60 meV), direct energy bandgap of 3.37 eV and rich morphological features (Umar and Hahn 2010; Umar 2017; Umar et al. 2011; Kumar et al. 2017a, b; Ajmal et al. 2019; Biswas et al. 2019; Huda et al. 2019). Nanoscale ZnO is studied widely for its potential technological applications, such as sensors, photocatalysis, UV lasers, solar cells, light emitting diodes arrays, and piezoelectric nanogenerators (Umar and Hahn 2010; Umar 2017; Umar et al. 2011, 2019 Kumar et al. 2014; Chaudhary et al. 2018; Chaudhary and Umar 2017; Wang 2004; Wang and Song 2006; Mao et al. 2019; Sannakashappanavar et al. 2019). Among several applications, ZnO has attracted more specifically, tremendous interest as photocatalyst for the degradation of several water pollutants due to its novel properties such as high photosensitivity, high photochemical stability, strong oxidation power, and non-toxicity (Djaja and Saleh 2013; Li et al. 2012; Trandafilovic et al. 2017; Li 2019; Siriwong et al. 2012). Further interest in this material is that it can be easily manipulated to form various morphologies with different sizes and intrinsic defect sites (oxygen vacancies and Zn interstitials) which are vital in influencing the photocatalytic and optical properties of ZnO nanomaterials (Zheng et al. 2007; Li and Haneda 2003; Xiong et al. 2006; Ishenko et al. 2005; Parangusan et al. 2019; Li and Su 2019; Ahmad et al. 2015). However, the role of the defects is also critical in that they restrain the recombination of photo-excited electron–hole (e^-–h^+) pair, facilitating their presence at the surface of the nanoparticle for catalytic performance (Zheng et al. 2007).

✉ Ahmad Umar
ahmadumar786@gmail.com

✉ M. S. Chauhan
mohinderc11@gmail.com

[1] Department of Chemistry, H. P. University, Gyan Path, Summer Hill, Shimla-5, India

[2] Department of Chemistry, Faculty of Science and Arts, Najran University, Najran 11001, Kingdom of Saudi Arabia

[3] Promising Centre for Sensors and Electronic Devices (PCSED), Najran University, Najran 11001, Kingdom of Saudi Arabia

Recently, there have been a profound interest expressed in tailoring the properties of nanoscale ZnO to enhance its functionalities by doping with selective impurities, especially with the rare-earth elements (Rodwihok et al. 2020; Kumar et al. 2020; An et al. 2019; Li 2019; Mao et al. 2019; Wang et al. 2018; Yang et al. 2018; Pan et al. 2019; Shabannia and Naderi 2019). Effect of doping with rare-earth elements, especially in moderate concentration, has been reported bring significant improvement in the photocatalytic and chemical sensing performances of nanosized ZnO (Kumar et al. 2015a, 2018; Chen et al. 2011; Nguyen et al. 2019). The detailed studies revealed that such dopant ions exist in the ZnO lattice in moderate concentration due to the difference in the charge and size, and induce defects, trapping the electrons, and suppressing the recombination of photo-generated (e^-–h^+) pairs due to electronic interaction between the valence band (VB) or conduction band (CB) of the host ZnO and the 4*f* and 5*d* states of the dopant ions, which resulted the enhanced photocatalytic performance of ZnO (Samadi et al. 2016; He et al. 2020). There have been various studies which report the synthesis of rare-earth doped ZnO nanomaterials and their photocatalytic and sensing applications (Kumar et al. 2015a, 2018; Chen et al. 2011; Nguyen et al. 2019; Aisah et al. 2017; Ziabari et al. 2019; Sin and Lam 2016).

Nguyen et al. (2019) investigated the photocatalytic degradation of MO dye using various concentrations (1–10 mol%) of La^{3+}-doped ZnO nanoparticles synthesized by sol–gel method under visible light illumination and found maximum decomposition with the sample doped with 10 mol% La^{3+}. Jian et al. (2009) studied the photocatalytic degradation properties of RhB dye using 1, 2, and 2.5 at% La^{3+}-doped ZnO nanowire synthesized via solvothermal process. Among all samples, the 2 at% La^{3+} was found to be the optimal doping content to achieve maximum degradation of RhB dye. Pascariu et al. (2019) have prepared various concentrations (0.02, 1, 2 and 4%) La^{3+}-doped ZnO nanostructures by electrospinning-calcination method and used for the photocatalytic degradation of Congo-Red (CR) dye under UV-light. Interestingly, the 2% La^{3+}-doped ZnO nanomaterials exhibited best photocatalytic performance among all samples towards the degradation of CR dye. La^{3+}-doped ZnO nanoparticles were also more effective photocatalytic antibacterial agent than pure ZnO because of the generation of more active oxygen species (Bomila et al. 2018). Thi and Lee (2017) reported on photocatalytic properties of ZnO nanoparticles under visible light when doped with 0.5, 1.0 and 1.5 wt% La using a facile precipitation method, and 1.0 wt% La doping showed the highest photocatalytic activity for the degradation of paracetamol.

In the present work, we report solution coprecipitation method to synthesis La^{3+}-doped ZnO nanoparticles. This is a most facile route through which morphology and the production of the material can be controlled merely via optimizing the experimental conditions such as pH, concentration of the precursors, temperature and the reaction time. The as-synthesized materials were used for the photocatalytic degradation of MO and Rh B dyes and PA under UV illumination. Further, fluorescence sensing studies of the as-prepared samples were also performed for the detection of PA in aqueous solution using Stern–Volmer model.

Material and methods

Zinc acetate, $(CH_3COO)_2Zn{\cdot}2H_2O$ was obtained from Merck, lanthanum acetate, La $(CH_3COO)_3{\cdot}xH_2O$ from CDH and PA, $(NO_2)_3C_6H_2OH$ from S.D. fine chemicals India Ltd. were all AR grade. Dyes, MO and Rh B were procured from MP Biomedicals. All solution preparations were made in doubly distilled water.

Synthesis of La-doped ZnO nanoparticles

In the synthesis procedure of ZnO nanoparticles, 100 mL of 75 mM aqueous solutions of NaOH was added dropwise into 100 mL 75 mM aqueous solution of $Zn(CH_3COO)_2{\cdot}2H_2O$ under continuous stirring condition. The pH of the resulting solution was brought to 11.5 by adding few drops of freshly prepared aqueous NaOH. The resulting solution was refluxed for 6 h at 95 °C, and the reaction mixture was allowed to attain room temperature. The white coloured precipitates so obtained were collected washed several times with distilled water and finally with ethanol, as reported (Kumar et al. 2020). However, the as-obtained material was dried in vacuum oven overnight and characterized by FTIR (Fourier-transform infrared) spectroscopy in terms of its compositional properties. In a typical procedure of nanocrystalline La-doped ZnO synthesis, 1, 5 and 10 mol % La doping was obtained by adding 100 mL of different contents of La $(CH_3COO)_3{\cdot}xH_2O$ aqueous solution into the 75 mM aqueous solutions of $Zn(CH_3COO)_2{\cdot}2H_2O$. To this reaction mixture was finally added 100 mL of 75 mM NaOH dropwise. The pH of this reaction mixture was also maintained as 11.5 and the reaction mixture refluxed for 6 h at 95 °C. As described previously, the materials obtained were washed with water and ethanol, and finally dried in vacuum oven before their characterization.

Characterizations

The crystallographic structure and lattice parameters of the as-synthesized materials were analysed through X-ray diffraction studies carried out at XRD; PANalyticalX'pert PRO with Cu-Kα radiations ($\lambda = 0.154$ nm) in the range of 10°–70° with scan speed of 4° min^{-1}. Morphological

characteristics and structures of nanomaterials were identified using NOVA NanoSEM field emission scanning electron microscope. Composition and purity of the as-synthesized nanostructures were established from EDX. Bandgap estimation was obtained from UV–Vis spectrophotometer (Varian Cary 100 Bio) in the range of 200–800 nm. The chemical compositions were examined by FTIR spectroscopy measured at room temperature in the range of 400–4000 cm^{-1}.

Photocatalytic activity

MO, RhB and PA were studied to evaluate the photocatalytic efficiency of the as-synthesized materials. 100 mg of ZnO and La^{3+}-doped ZnO were dispersed in 100 mL of 10 ppm aqueous solution of target species, i.e. MO, RhB and PA. Each system was stirred for about 90 min in dark atmosphere to ensure adsorption–desorption of these target species at the surface of photocatalyst established. After stirring in dark, each system was subjected to UV-light illumination from 125 W high pressure mercury vapour lamp. 3 mL of each reaction system was taken at regular time intervals and absorption spectra recorded at $\lambda_{max} = 464$, 554 and 355 nm for MO, RhB and PA, respectively. Decrease in the absorbance value with the increase in UV illumination time as recorded from UV spectrophotometer inferred the decomposition of these species.

Fluorescent sensing properties

The fluorescent (FL) measurements were performed at room temperature using Perkin Elmer LS-55 fluorescence spectrophotometer to investigate the sensing ability of these materials for PA in aqueous solution. Each experiment was performed with 1 mg of the as-synthesized nanomaterials taken in 50 mL aqueous solution and sonicated to ensure their well-dispersion. The FL measurements were carried out with the excitation wavelength of 380 nm for pure ZnO and 385 nm for 1, 5 and 10 mol % La-doped ZnO nanoparticles. The sensing experiments were performed with 5 mM PA solution added in successive instalments of 0.5 µL to each suspension and FL spectrum recorded after each addition at their respective excitation wavelength.

Results and discussion

The crystal properties and phases of the synthesized La-doped ZnO nanoparticles were studied by X-ray diffraction and results are shown in Fig. 1. Various diffraction peaks appeared in the XRD patterns at $2\theta = 31.8°$, 34.4°, 36.3°, 47.6°, 56.7°, 62.9°, 66.3°, 68.0° and 69.2° are in according to the pure wurtzite hexagonal crystal structure of ZnO (Umar et al. 2011, 2019). The observed diffraction peaks are assigned

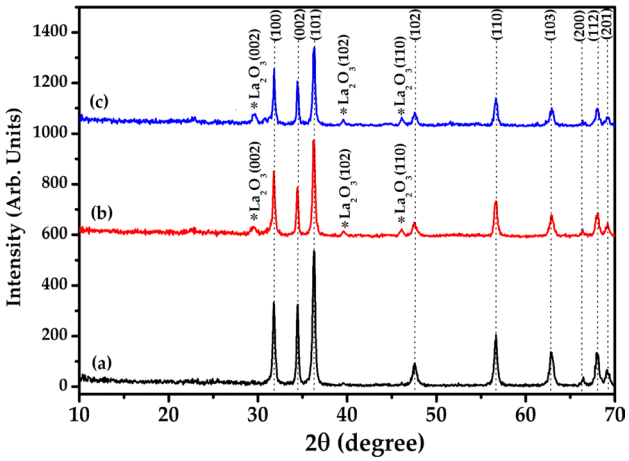

Fig. 1 Typical XRD pattern of the as-synthesized La-doped ZnO nanoparticles; **a** 1 mol% La^{3+}, **b** 5 mol% La^{3+} and **c** 10 mol% La^{3+}

as ZnO (100), (002), (101), (102), (110), (103), (200), (112) and (201) which are well-matched with the reported literature and JCPDS card no. 36-1451 for ZnO (Umar et al. 2011, 2019; Kumar et al. 2015a, b). In addition to these ZnO peaks, three small peaks appeared at $2\theta = 29.1°$, 39.5° and 45.3° in 5 and 10 mol% La-doped ZnO which can be assigned as La_2O_3 (002), La_2O_3 (102) and La_2O_3 (110). The observed diffraction peaks related with La_2O_3 is well-matched with the reported literature (Umar et al. 2020). No apparent peak related with La and related phases were observed in the XRD pattern of 1 mol% La-doped ZnO which clearly revealed that due to low-concentration of La, it is homogeneously dispersed into the lattices of ZnO without inducing deformation in the crystal structure of ZnO.

Hence, in the present study, the 1 mol% La^{3+} ions successfully incorporated into the crystal lattices of ZnO without affecting much of its crystallographic quality. Additionally, the peak intensities are observed to decrease and broadened after doping, indicating decrease in the crystallinity of ZnO due to the dispersion of dopant ions (Gobbo et al. 2020; Shakir et al. 2016). The lattice parameters and crystallite size of the synthesized La-doped ZnO nanoparticles were calculated from the Debye–Scherrer formula (He et al. 2018; Chen et al. 2011; Nguyen et al. 2019; He 2017) and results are summarized in Table 1. Interestingly at lower La^{3+} ions concentration, the crystalline size was higher; however, with increasing the La^{3+} ions concentrations (5 and 10 mol%), the crystalline size was decreased. The observed results are well-consistent with the previous report (He et al. 2015):

$$\frac{1}{d^2} = \frac{4}{3}\left[\frac{h^2 + hk + k^2}{a^2}\right] + \frac{l^2}{c^2}.$$

Figure 2a, c, e depicts the typical FESEM images of the as-synthesized 1 mol%, 5 mol% and 10 mol% La-doped

Table 1 Lattice parameters of La-doped ZnO nanostructures

La-doped ZnO nanoparticles	Lattice parameters (Å)		Crystalline size (nm)
	a	*c*	
1 mol% La-doped ZnO	3.2508	5.2113	26.61
5 mol% La-doped ZnO	3.2509	5.2132	19.61
10 mol% La-doped ZnO	3.2477	5.2091	20.12

ZnO materials, respectively. The FESEM images revealed the high-density growth of nanodimensional particles, thus called it as, "nanoparticles". Most of the nanoparticles possess cone-shaped morphologies; however, some spherical nanoparticles are also seen in the micrographs. Furthermore, due to high-density growth, some agglomeration in the nanoparticles were also seen. The typical sizes of the nanoparticles are in the range of 35 ± 10 nm.

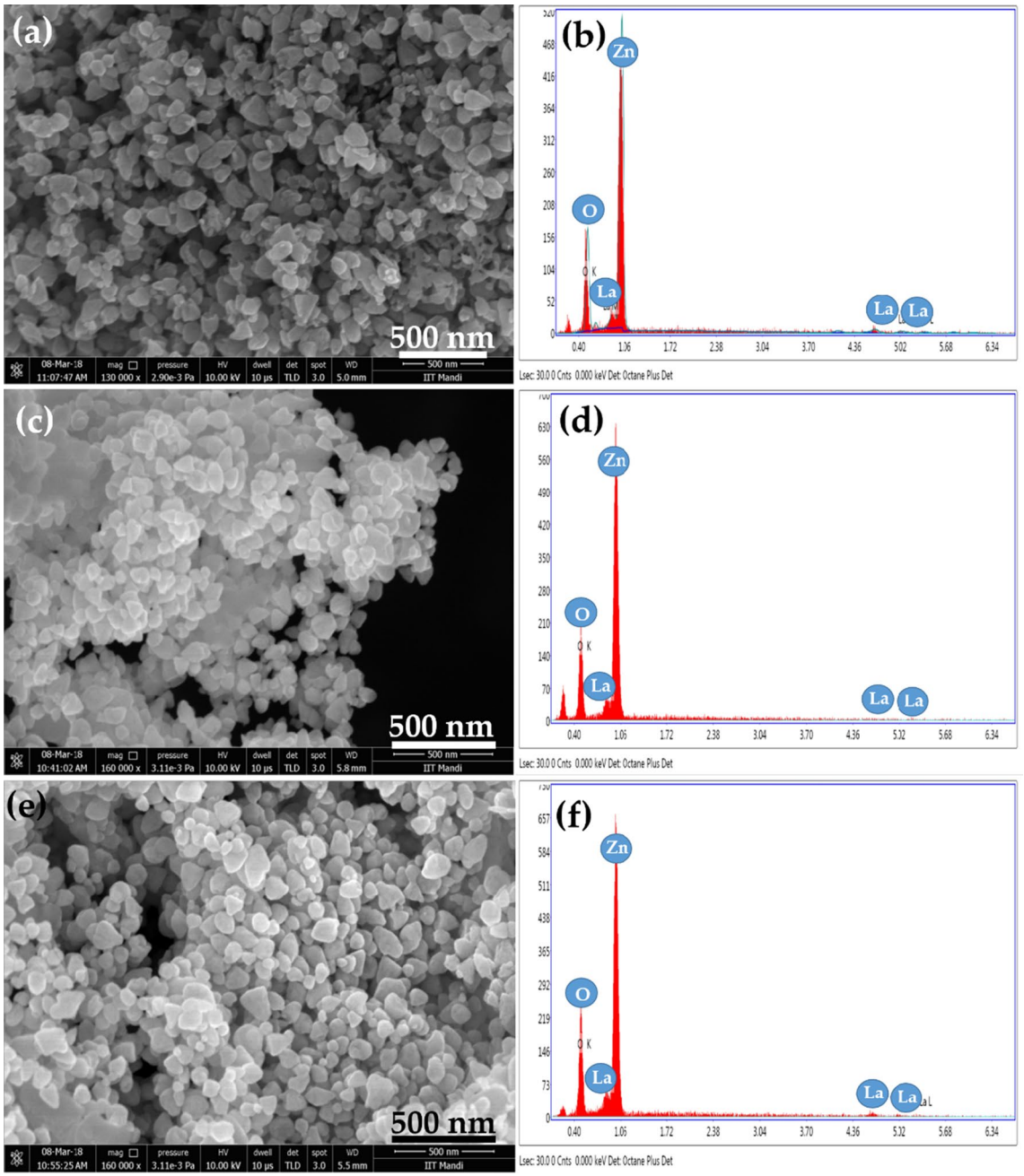

Fig. 2 Typical FESEM images of **a** 1 mol%, **c** 5 mol% and **e** 10 mol% of La-doped ZnO nanoparticles and **b**, **d**, **f** their corresponding EDS spectra, respectively

The elemental compositions of the synthesized La-doped ZnO nanoparticles were examined by energy dispersive spectroscopy (EDS). Figure 2b, d, f exhibits the typical EDS spectrum of the as-synthesized 1 mol%, 5 mol% and 10 mol% La-doped ZnO nanoparticles, respectively. As can be seen from the observed EDS spectra that all the synthesized nanoparticles are significantly made of zinc (Zn), oxygen (O) and lanthanum (La) only. No other impurity was detected in the observed EDS spectra which clearly revealed that the synthesized materials are La-doped ZnO.

The optical properties of the synthesized La-doped ZnO nanoparticles were studied by UV–visible spectroscopy at room temperature. UV–Vis absorption spectra of the as-prepared La-doped ZnO nanoparticles are shown in Fig. 3. As seen there was a single well-defined peak that appeared at 375, 378 and 376 nm for 1, 5 and 10 mol% La^{3+}-doped ZnO nanoparticles, respectively. Interestingly, all these values are very close to the characteristic value of well-crystalline wurtzite hexagonal phase of ZnO (Al-Hadeethi et al. 2018, 2019; Biswas et al. 2019; Umar et al. 2011; Yang et al. 2018; Kumar et al. 2018).

This while indicates no effect of dopant on the particle size of ZnO, is suggested to imply that La^{3+} ions tend to occupy the interstitial voids of ZnO lattice without affecting much of its size. The corresponding electronic energy bandgap (E_g) was obtained from the following relation (Al-Hadeethi et al. 2018, 2019; Arin et al. 2014; Biswas et al. 2019; Umar et al. 2011; Yang et al. 2018):

$$E_g = \frac{1240}{\lambda},$$

where λ corresponds to λ_{max} as estimated above. The E_g values were found to be 3.30, 3.28 and 3.30 eV for 1, 5 and 10 mol% La-doped ZnO nanoparticles, respectively, suggesting these materials to be UV responsive.

Figure 4 depicts the FTIR spectra of pure ZnO and 1, 5 and 10 mol% La-doped ZnO nanoparticles at room temperature in the range of 400–4000 cm^{-1}. The observed FTIR spectra exhibited several well-defined peaks which are assigned according to their corresponding wave numbers. A common peak for all the four samples existing at 479 cm^{-1} is due to stretching mode for Zn–O bond (Al-Hadeethi et al. 2018, 2019; Biswas et al. 2019; Umar et al. 2011). The peaks observed in the region 860–900 are due to O–Zn–O stretching and exhibit the formation of tetrahedral coordinated Zn (Arin et al. 2014). Peaks observed in the 3400–3650 cm^{-1} region and around 2362 cm^{-1} are ascribed to O–H stretching mode, which might be appearing due to moisture adsorbed on the surface of nanostructures (Al-Hadeethi et al. 2018, 2019; Biswas et al. 2019; Umar et al. 2011). Bands appearing around 3000 cm^{-1} might be due to C–H stretching of CH_3 probably from the acetate precursors used in synthesis of these nanostructures. Peaks observed in the region 1500–1700 cm^{-1} are due to symmetric and asymmetric stretching vibrations of C=O functional group (Yayapao et al. 2013). Peaks around 1150 cm^{-1} can be attributed to C–C bonds.

It can be seen from the figure that peaks from CH_3 and COOH groups are more pronounced for La-doped ZnO as

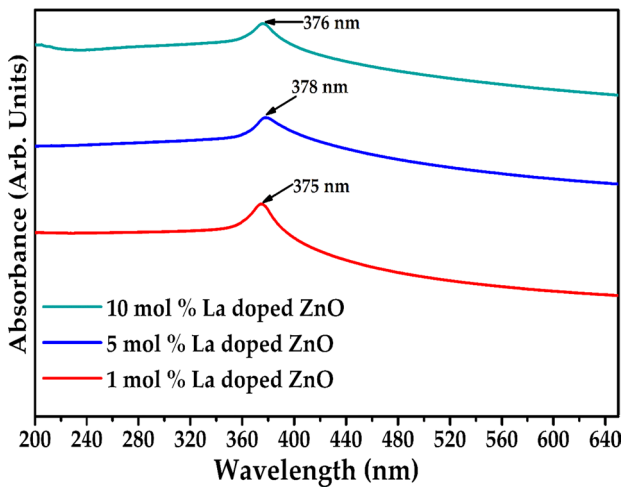

Fig. 3 Typical UV–Vis. spectra of 1 mol%, 5 mol% and 10 mol% La-doped ZnO nanoparticles

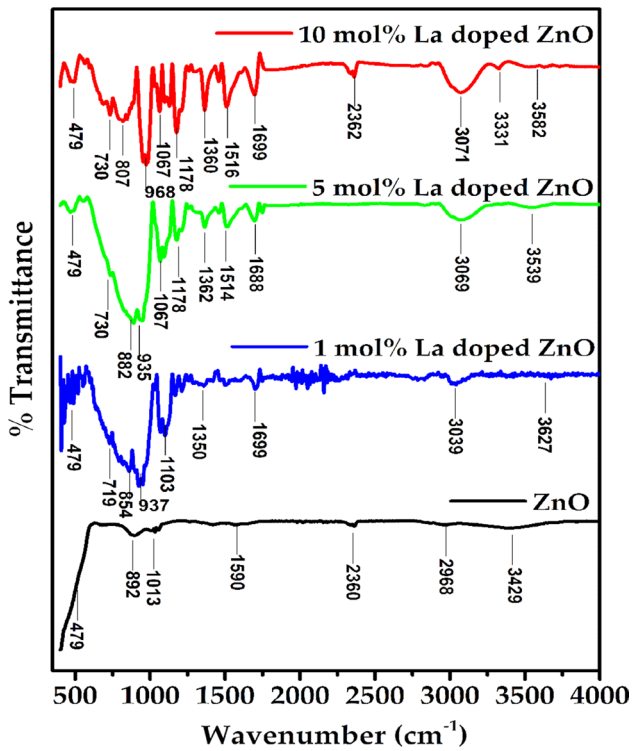

Fig. 4 FTIR spectra of ZnO, 1 mol%, 5 mol% and 10 mol% of La-doped ZnO nanoparticles

compared to undoped ZnO, which is indicating the presence of higher amounts of acetate in these samples (Nguyen et al. 2019; Aisah et al. 2017). Peaks centred around 1360 cm^{-1} are ascribed to hydrogen related defects on the surface of ZnO nanostructures (Al-Hadeethi et al. 2018, 2019; Biswas et al. 2019; Umar et al. 2011).

The representative results for the photodegradation process of MO, RhB and PA as inferred from decolouration of their aqueous solutions with the increase in time of UV illumination in the presence of catalyst is depicted in Fig. 5.

Figure 5 demonstrates the representative time-dependent UV–Vis. absorption spectra of three different dyes, i.e. MO, RhB and PA in presence of 1 mol% La-doped ZnO nanoparticles at different time of UV illumination. The decomposition of different dyes was observed by monitoring the change in the absorption intensity of the corresponding absorption peaks for particular dye. Interestingly, with increasing irradiation time in presence of catalyst, the absorption intensity decreases which confirms that the synthesized La-doped ZnO nanoparticles are effective photocatalysts for the photocatalytic degradation of various organic dyes such as MO, RhB and PA.

The extent of degradation of these target organic dyes such as MO, RhB and PA was calculated from the below-mentioned relation:

$$\text{Degradation}\,(\%) = \left[\left(A_0 - A\right)/A_0\right] \times 100,$$

where A_0 and A refer to absorption intensity of the reaction system at '0' and 't' time of UV exposure.

Figure 6 exhibits the typical graph for % degradation of various organic dyes, i.e. MO, RhB and PA as a function of irradiation time (min) in the absence and presence of various photocatalysts such as ZnO, 1, 5 and 10 mol% La-doped ZnO. The results indicating the effect of dopant concentration on photodegradation of MO, Rh B and PA after 180 min under UV illumination.

It can be seen that ~ 60–75% of these target species are degraded over a period of 180 min of UV illumination in the presence of pure ZnO, while almost 95–100% degradation occurred with 1 mol% La-doped ZnO in 120 min. This turned out to be the best photocatalyst among the as-synthesized materials.

Further, the rate of photodegradation of MO, RhB and PA in their aqueous solutions was studied using Langmuir–Hinshelwood model (Kumar et al. 2020):

$$-\ln\left(C/C_0\right) = kt,$$

where C_0 is the initial concentration of dye molecules, C is the concentration at various time intervals 't' and k is apparent first-order rate constant. A linear dependence was observed in each case when $-\ln(C/C_0)$ was plotted against time 't' (Fig. 7). The degradation rate constant values as calculated from least-squares fitting of the data are presented in Table 2. As revealed, maximum photocatalytic activity is achieved for MO, Rh B and PA degradation while using 1 mol% La-doped ZnO catalyst.

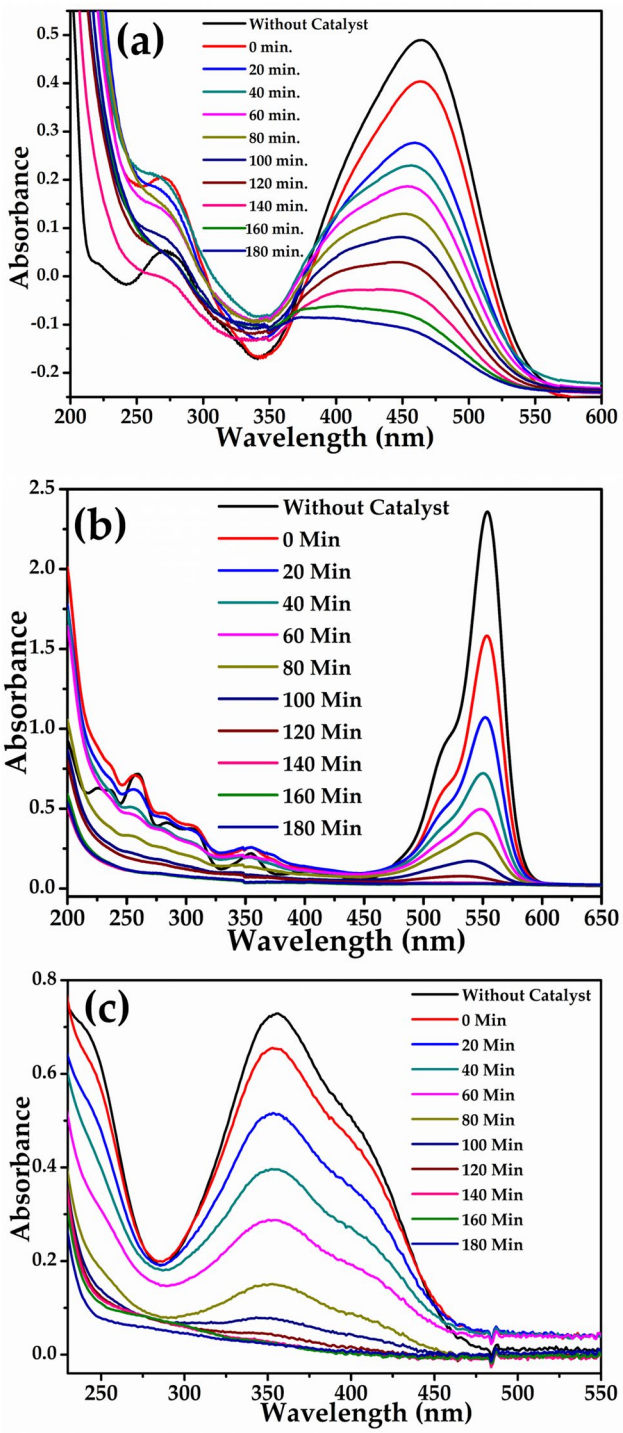

Fig. 5 UV–Vis spectra of **a** MO, **b** Rh B and **c** PA in the presence of 1 mol% La-doped ZnO at different time of UV illumination

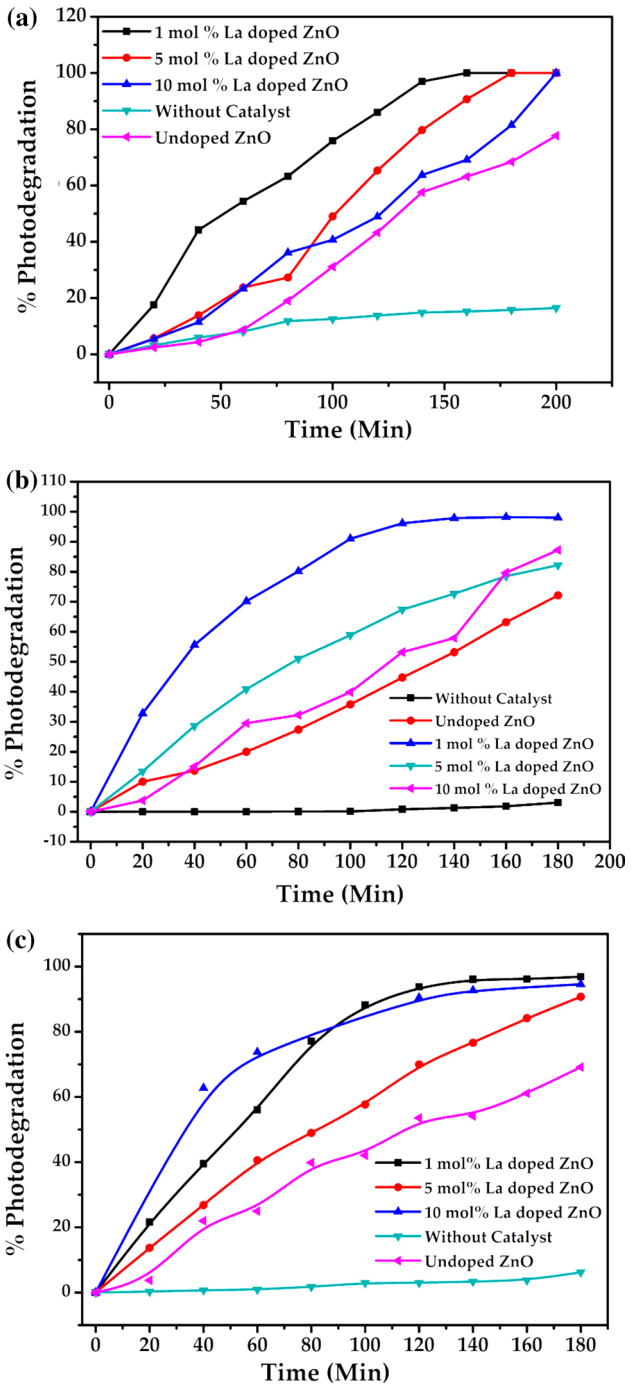

Fig. 6 Progress of photodegradation of **a** MO, **b** RhB and **c** PA in the presence of the as-fabricated photocatalysts

The XRD results revealed that the 1 mol% La^{3+} ions are successfully doped into the lattices of ZnO without significantly changing the crystal structure of the parental material which most probably led the La^{3+} ions to function as an effective trap for photo-excited electrons. As a result, the electron–hole recombination is inhibited, and higher photocatalytic efficiency achieved. However, because of the stable noble gas (Xe) configuration of La^{3+}, the trapped electron can easily be transferred to the most abundant bulk ionized oxygen vacancy defects of ZnO, and so on reacting with adsorbed O_2 formed oxide radical, O_2^- which led to the formation of highly reactive hydroxyl radical (·OH) (Sin and Lam 2016; Rostami 2017). Likewise, holes are also expected to generate ·OH radicals while reacting with ionized oxygen, interstitial and/or with surface adsorbed water molecules (Sin and Lam 2016). Moreover the 1 mol% La-doped ZnO nanoparticles exhibited the highest photocatalytic activity compared to the other samples for the degradation of dyes and PA which is consistent with the photocatalytic results as reported by various workers (Pascariu et al. 2019; Thi and Lee 2017; Jian et al. 2009; Nguyen et al. 2019) Above 1 mol% dopant concentration as La^{3+} secondary phase begins to appear, as noted from the XRD results, it suggests that all amounts of the dopant are not incorporated into the ZnO lattice. Because of this, surface adsorbed oxygen concentration is reduced, which would otherwise be expected used for the generation of superoxide ion O_2^-. Thus the charge pair separation is inhibited and photocatalytic efficiency decreased. Moreover, appearance of second phase with 5 and 10 mol% La doping can also be viewed as enabling the aggregation of nanoparticles that subsequently reduced the surface area of the nanoparticles as well. To study the sensing property of the as-synthesized ZnO and La-doped ZnO nanoparticles towards PA, Stern–Volmer equation (Eq. 1) (Singh and Mehta 2016) was employed.

$$I_o/I = 1 + K_{sv}[Q], \tag{1}$$

where 'I_o' and 'I', respectively, refer to the fluorescence intensity in the absence and in the presence of quencher (PA) of concentration [Q] and K_{sv} is the Stern–Volmer quenching constant.

Figure 8 shows the decrease in the FL intensity with the increase in the concentration of the quencher (PA). This can be attributed to the association of PA on the surface of the photoluminescent sensor (La-doped ZnO) which traps the excited electron successively with the increase in quencher (PA) concentration through charge transfer mechanism (Toal and Trogler 2006). These results when analysed in terms of Eq. (1) are presented in Fig. 9. A linear dependence between ($I_o/I - 1$) and [Q] was observed in all the cases over the [Q] < 4–5 μM with regression coefficient, R found to lie in the range 0.9783–0.9951 and slope (Stern–Volmer constant) K_{sv} as 504,250, 287,120, 505,560 and 389,630 M^{-1}, respectively, for ZnO, 1, 5 and 10 mol % La-doped ZnO.

This is suggested to sense static quenching (Singh and Mehta 2016), while a non-linear trend displayed above the 4–5 μM concentration of the quencher allowed the identification of co-existence of static and dynamic quenching by PA (Singh and Mehta 2016). The entire experimental data

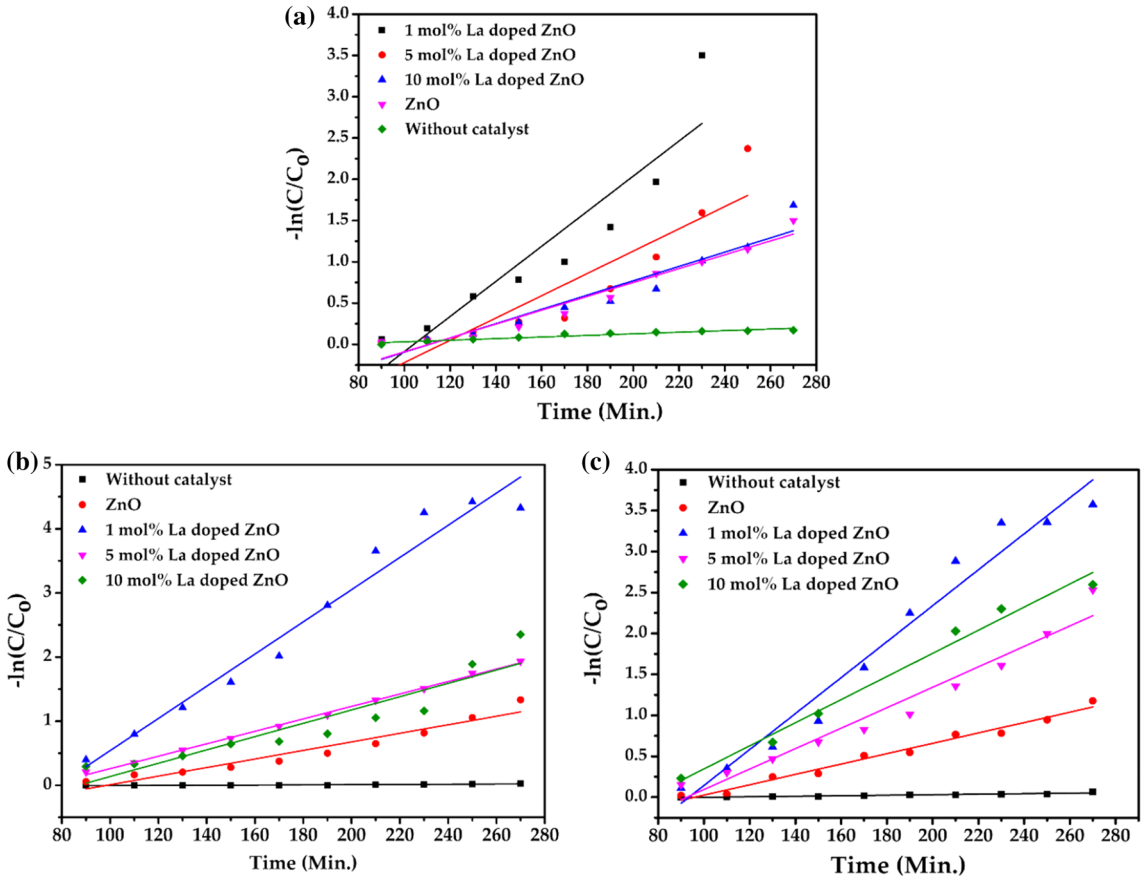

Fig. 7 Kinetics of degradation for **a** MO, **b** RhB and **c** PA

Table 2 Photodegradation rate constant k, min^{-1}

Photocatalyst	k, min^{-1}		
	MO	Rh B	PA
Blank	9.56×10^{-4}	1.48×10^{-4}	3.14×10^{-4}
ZnO	8.4×10^{-3}	6.68×10^{-3}	6.49×10^{-3}
1 mol% La-doped ZnO	2.14×10^{-2}	2.51×10^{-2}	2.19×10^{-2}
5 mol% La-doped ZnO	1.36×10^{-2}	0.971×10^{-2}	1.84×10^{-2}
10 mol% La-doped ZnO	0.872×10^{-2}	1.03×10^{-2}	1.41×10^{-2}

were subsequently subjected to the analysis in terms of the Stern–Volmer equation in its modified form (Eq. 2) (Singh and Mehta 2016):

$$\frac{I_o - I}{Ie^{V[Q]}} = K_{sv}[Q], \tag{2}$$

where V is the static quenching constant obtained from Eq. (2). Plotting $\frac{I_o - I}{Ie^{V[Q]}}$ against $[Q]$ was performed with varying V until a linear response is achieved (Fig. 9). The value of K_{sv} values thus obtained with regression coefficient, R in the range 0.9183–0.9827 were as 647,560, 214,350, 250,260 and 167,520, respectively, for ZnO (Kumar et al. 2020), 1, 5 and 10 mol% La-doped ZnO. As these K_{sv} values are found to be lower than that of obtained for static quenching, (except pure ZnO), it is inferred that below ~ 5 µM concentration of PA, there exists strong binding, and hence quenching is expected to have occurred due to the complexation between La-doped ZnO nanoparticles and PA, while at higher concentration, a competition is likely to have existed between the dynamic and static binding of PA with nanoparticles.

The limit of detection for ZnO and 1, 5 and 10 mol% La-doped ZnO towards PA in aqueous solutions was obtained from these plots according to 3σ/m rule (Toal and Trogler

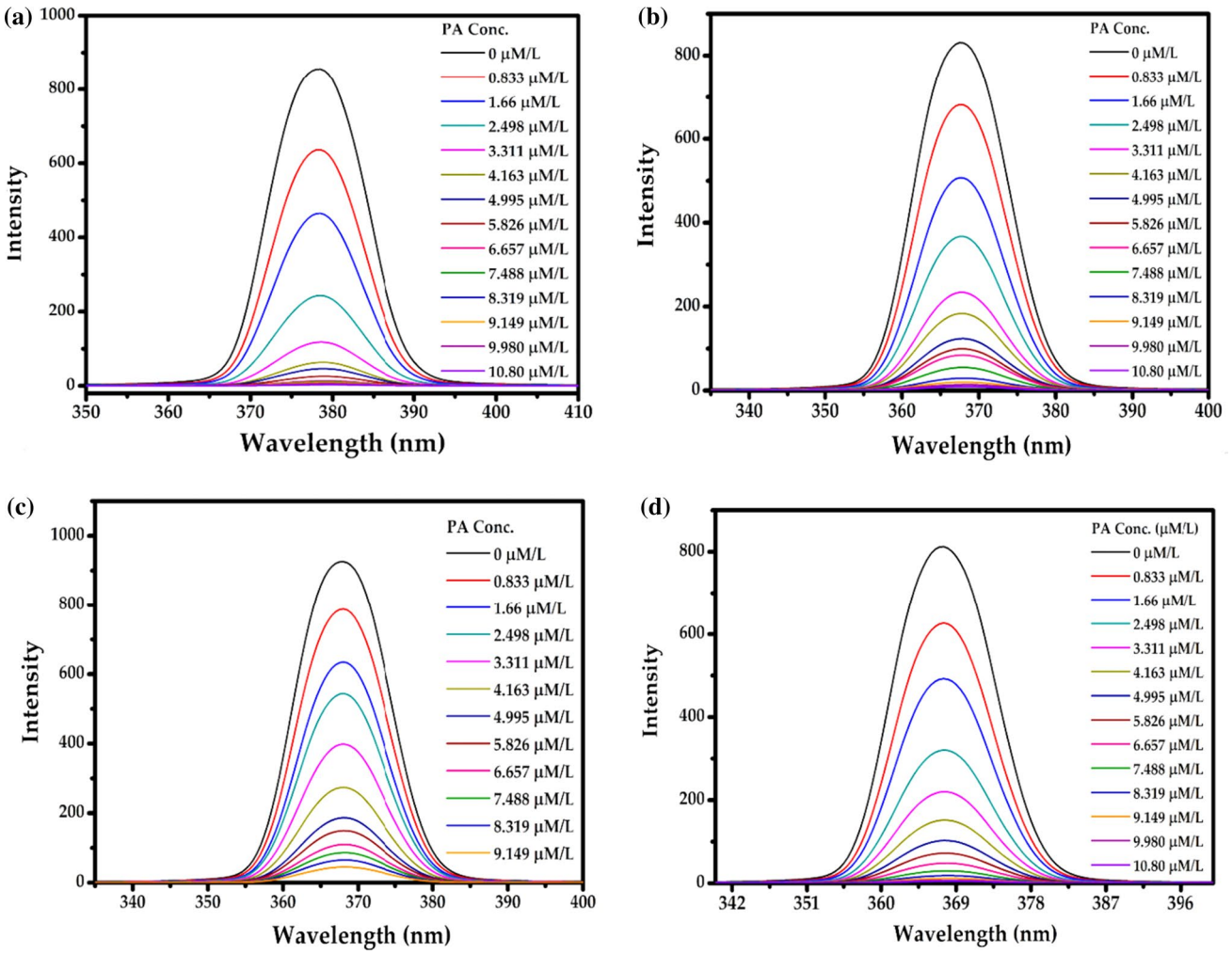

Fig. 8 Variation of PL intensity of **a** ZnO, **b** 1 mol%, **c** 5 mol% and **d** 10 mol% La-doped ZnO with the addition of PA

2006; Singh and Mehta 2016) and was found to be, respectively, 2.89 (Kumar et al. 2020), 1.05, 1.38 and 1.38 µM L^{-1}. Interestingly, 1 mol% La-doped ZnO nanomaterial was found to be the most sensitive for the detection of PA.

Conclusions

The ZnO and La-doped ZnO nanoparticles synthesized using simple solution precipitation method have been studied for the photocatalytic degradation of MO, Rh B dyes and PA under UV illumination. As confirmed from the XRD results, the 1 mol% La^{3+} ions successfully incorporated into the crystal lattices of ZnO without affecting much of its crystallographic quality. Interestingly, the 1 mol% La-doped ZnO nanoparticles were found to be most efficient photocatalyst towards the degradation of MO, Rh B and PA dyes and also for the fluorescent detection of PA in aqueous solution. The observed results revealed that the La-doped ZnO nanomaterials are potential scaffold for the enhanced photocatalytic and sensing applications.

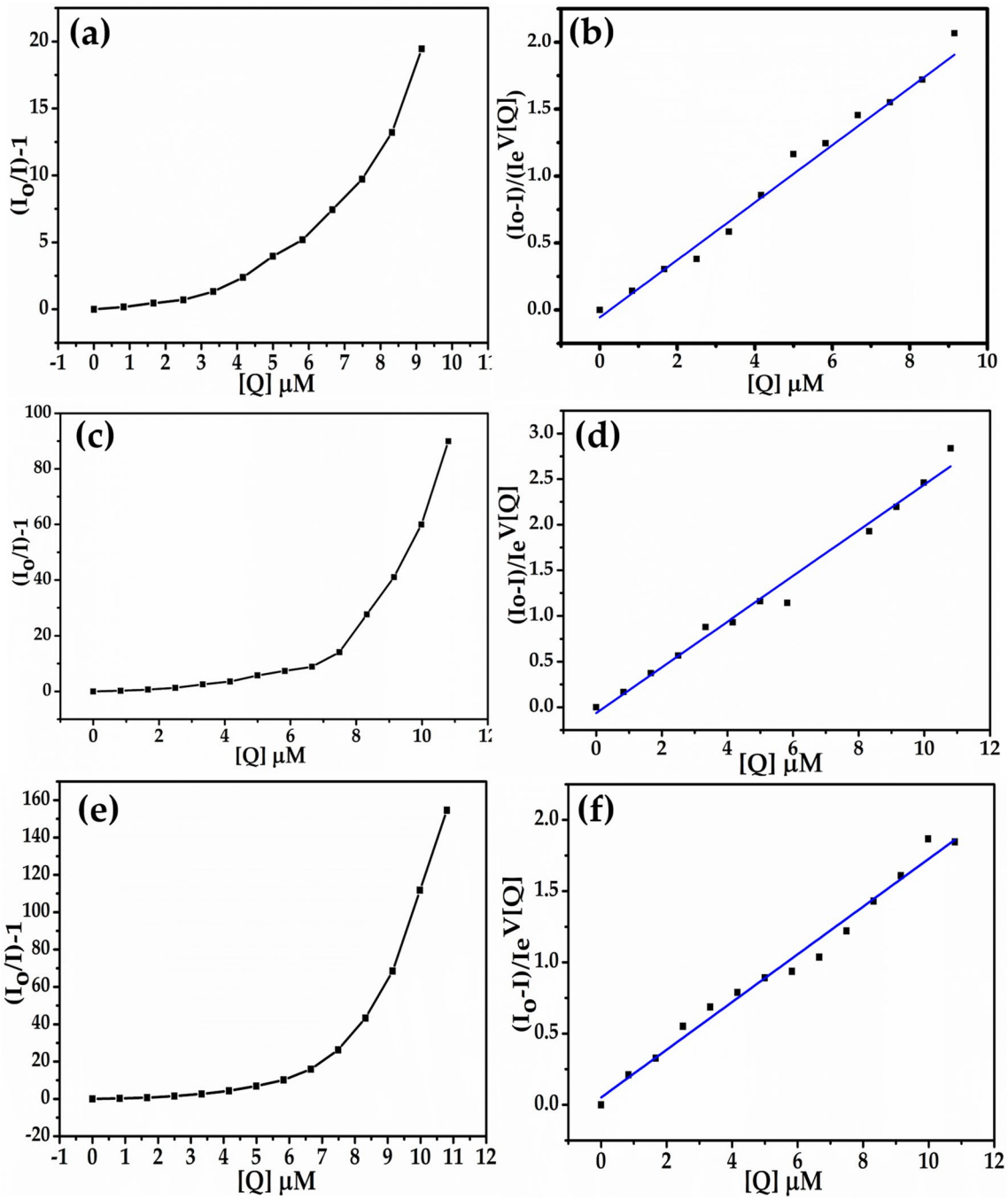

Fig. 9 Stern–Volmer plots for 1 mol% (**a**, **b**), 5 mol% (**c**, **d**) and 10 mol% (**e**, **f**) La-doped ZnO nanoparticles

Acknowledgements Manoj Kumar thanks UGC, New Delhi for the award of SRF. Instrument grant sanctioned to the Chemistry Department H. P. University Shimla by UGC under UGC-SAP is gratefully acknowledged. Ahmad Umar would like to acknowledge Najran University and Ministry of Education, Kingdom of Saudi Arabia for support.

References

Ahmad M, Ahmed E, Zafar F, Khalid NR, Niaz NA, Hafeez A, Ikram M, Khan MA, Zhanglian H (2015) Enhanced photocatalytic activity of Ce-doped ZnO nanopowders synthesized by combustion method. J Rare Earths 33(3):255–262. https://doi.org/10.1016/S1002-0721(14)60412-9

Aisah N, Gustiono D, Fauzia V, Sugihartono I, Nuryadi R (2017) Synthesis and enhanced photocatalytic activity of Ce-doped zinc oxide nanorods by hydrothermal method. IOP Conf Ser Mater Sci Eng. https://doi.org/10.1088/1757-899X/172/1/012037

Ajmal HMS, Khan W, Khan F, Huda NU, Kim SD (2019) Hydrothermally grown copper-doped ZnO nanorods on flexible substrate. J Nanoelectron Optoelectron 14:1503–1511. https://doi.org/10.1166/jno.2019.2639

Al-Hadeethi Y, Umar A, Ibrahim AA, Kumar R, Al-Heniti SH, Raffah BM (2018) Hydroquinone sensor based on neodymium (Nd) doped ZnO hexagonal nanorods. Nanosci Nanotechnol Lett 10:351–357. https://doi.org/10.1166/nnl.2018.2620

Al-Hadeethi Y, Umar A, Singh K, Ibrahim AA, Al-Heniti SH, Raffah BM (2019) Ytterbium-doped ZnO flowers based phenyl hydrazine chemical sensor. J Nanosci Nanotechnol 19:4199–4204. https://doi.org/10.1166/jnn.2019.16283

An X, Guo S, Su J, Hu Q, Zhu W, Liu L, Zhang Y, Liu G (2019) Enhanced ethanol sensing performance of ZnO–SnO_2 heterostructure nanotubes. Sci Adv Mater 11:360–365. https://doi.org/10.1166/sam.2019.3466

Arin J, Dumrongrojthanath P, Yayapao O, Phuruangrat A, Thongtem S, Thongtem T (2014) Synthesis, characterization and optical activity of La-doped $ZnWO_4$ nanorods by hydrothermal method. Superlattices Microstruct 67:197–206. https://doi.org/10.1016/j.spmi.2013.12.024

Biswas R, Roy T, Chatterjee S (2019) Study of electro-optical performance and interfacial charge transfer dynamics of dye sensitized solar cells based on ZnO nanostructures and natural dyes. J Nanoelectron Optoelectron 14:99–108. https://doi.org/10.1166/jno.2019.2445

Bomila R, Srinivasan S, Gunasekaran S, Manikandan A (2018) Enhanced photocatalytic degradation of methylene blue dye, opto-magnetic and antibacterial behaviour of pure and La—doped ZnO nanoparticles. J Supercond Nov Magn 31:855–861. https://doi.org/10.1007/s10948-017-4261-8

Chaudhary S, Umar A (2017) ZnO nanostructures and their sensing applications: a review. Nanosci Nanotechnol Lett 9:1787–1826. https://doi.org/10.1166/nnl.2017.2579

Chaudhary S, Umar A, Bhasin KK, Baskoutas S (2018) Chemical sensing applications of ZnO nanomaterials. Materials 11:287. https://doi.org/10.3390/ma11020287

Chen XY, Fang F, Ng AMC, Djurisic AB, Chan WK, Lui HF, Fong PWK, Surya C, Cheah KW (2011) Effect of doping precursors on the optical properties of Ce-doped ZnO nanorods. Thin Solid Films 520:1125–1130. https://doi.org/10.1016/j.tsf.2011.08.022

Djaja NF, Saleh R (2013) Characterization and photocatalytic activities of Ce doped ZnO nanoparticles. Mater Sci Appl 4:145–152. https://doi.org/10.4236/msa.2013.42017

Gobbo SD, Poolwong J, D'Elia V, Ogawa M (2020) Simultaneous controlled seeded-growth and doping of ZnO nanorods with aluminum and cerium: feasibility assessment and effect on photocatalytic activity. Cryst Growth Des 20:5508–5525. https://doi.org/10.1021/acs.cgd.0c00694

He HY (2017) Photocatalytic activity of reduced graphene oxide-SnSe nanohybrids with efficiency interface effect. NANO. https://doi.org/10.1142/S1793292017500321

He HY, Huang J, Fei J, Lu J (2015) La-doping content effect on the optical and electrical properties of La-doped ZnO thin films. J Mater Sci Mater Electron 26:1205–1211. https://doi.org/10.1007/s10854-014-2526-6

He HY, He Z, Shen Q (2018) Efficient hydrogen evolution catalytic activity of graphene/metallic MoS2 nanosheet heterostructures synthesized by a one-step hydrothermal process. Int J Hydrog Energy 43(48):21835–21843. https://doi.org/10.1016/j.ijhydene.2018.10.023

He L, Meng J, Feng J, Yao F, Zhang L, Zhang Z, Liu X, Zhang H (2020) Investigation of 4*f*-related electronic transitions of rare-earth doped ZnO luminescent materials: insights from first-principles calculations. ChemPhysChem 21(1):51–58. https://doi.org/10.1002/cphc.201900981

Huda NU, Khan F, Ajmal HMS, Khan W, Kim SD (2019) Influence of the N_2O plasma treated ZnO seed crystallites on opto-electrical properties of hydrothermally grown ZnO nanorods on plastic substrate. J Nanoelectron Optoelectron 14:1358–1367. https://doi.org/10.1166/jno.2019.2602

Ishenko V, Polarz S, Grote D, Stavarache V, Fink K, Driess M (2005) Zinc oxide nanoparticles with defects. Adv Funct Mater 15:1945–1954. https://doi.org/10.1002/adfm.200500087

Jian T, Wang W, Long F, Fu Z, Wang H, Zhang Q (2009) Fabrication, characterization and photocatalytic activity of La-doped ZnO nanowires. J Alloy Compd 484:410–415. https://doi.org/10.1016/j.jallcom.2009.04.153

Kumar R, Kumar G, Umar A (2014) Zinc oxide nanomaterials for photocatalytic degradation of methyl orange: a review. Nanosci Nanotechnol Lett 6:631–650. https://doi.org/10.1166/nnl.2014.1879

Kumar R, Al-Dossary O, Kumar G, Umar A (2015a) Zinc oxide nanostructures for NO_2 gas sensor applications: a review. Nano Micro Lett 7:97–120. https://doi.org/10.1007/s40820-014-0023-3

Kumar R, Rana D, Umar A, Sharma P, Chauhan S, Chauhan MS (2015b) Ag-doped ZnO nanoellipsoids: potential scaffold for photocatalytic and sensing applications. Talanta 137:204–213. https://doi.org/10.1016/j.talanta.2015.01.039

Kumar R, Umar A, Kumar G, Nalwa HS (2017a) Antimicrobial properties of ZnO nanomaterials: a review. Ceram Int 43:3940–3961. https://doi.org/10.1016/j.ceramint.2016.12.062

Kumar R, Umar A, Kumar G, Nalwa HS, Kumar A, Akhtar MS (2017b) Zinc oxide nanostructure based dye sensitized solar cells. J Mater Sci 52:4743–4795. https://doi.org/10.1007/s10853-016-0668-z

Kumar DR, Ranjith KS, Kumar RTR (2018) Structural, optical, photocurrent and solar driven photocatalytic properties of vertically aligned samarium doped ZnO nanorod arrays. Optik 154:115–125. https://doi.org/10.1016/j.ijleo.2017.10.004

Kumar M, Chauhan MS, Shaheer Akhtar M, Umar A (2020) Effect of cerium ions in Ce-Doped ZnO nanostructures on their photocatalytic and picric acid chemical sensing. Ceram Int. https://doi.org/10.1016/j.ceramint.2020.09.145

Li Z (2019) Study for the structure and optical properties of ZnO microstructures prepared by chemical vapor deposition method. Sci Adv Mater 11:1168–1173. https://doi.org/10.1166/sam.2019.3525

Li D, Haneda H (2003) Morphologies of zinc oxide particles and their effects on photocatalysis. Chemosphere 51:129–137. https://doi.org/10.1016/s0045-6535(02)00787-7

Li SS, Su YK (2019) Improvement of the performance in Cr-doped ZnO memory devices via control of oxygen defects. RSC Adv 9:2941–2947. https://doi.org/10.1039/C8RA10112D

Li B, Liu T, Wang Y, Wang Z (2012) ZnO/graphene-oxide nanocomposites with remarkably enhanced visible-light-driven photocatalytic performance. J Colloid Interface Sci 377:114–121. https://doi.org/10.1016/j.jcis.2012.03.060

Mao Y, Zhang W, Wang Y, Guan R, Liu B, Wang X, Sun Z, Xing L, Chen S, Xue X (2019) Self-powered wearable athletics monitoring nanodevice based on ZnO nanowire piezoelectric-biosensing unit arrays. Sci Adv Mater 11:351–359. https://doi.org/10.1166/sam.2019.3447

Nguyen LTT, Nguyen LTH, Duong ATT, Nguyen BD, Hai NQ, Chu VH, Nguyen TD, Bach LG (2019) Preparation, characterization and photocatalytic activity of La-doped zinc oxide nanoparticles. Materials 12:1195–1205. https://doi.org/10.3390/ma12081195

Pan X, Cheng L, Chen L, Li H, Zhou J, Xie E (2019) A wire-like UV detector based on TiO_2-coated ZnO nanotube arrays. Sci Adv Mater 11:392–395. https://doi.org/10.1166/sam.2019.3451

Parangusan H, Ponnamma D, Al-Maadeed MAA (2019) Effect of cerium doping on the optical and photocatalytic properties of ZnO nanoflowers. Bull Mater Sci 42:179–189. https://doi.org/10.1007/s12034-019-1865-6

Pascariu P, Homocianu M, Cojocaru C, Samoila P, Airinei A, Suchea M (2019) Preparation of La doped ZnO ceramic nanostructures by electrospinning-calcination method: effect of La^{3+} doping on optical and photocatalytic properties. Appl Surf Sci 476:16–27. https://doi.org/10.1016/j.apsusc.2019.01.077

Rodwihok C, Wongratanaphisan D, Van Tam T, Choi WM, Hur SH, Chung JS (2020) Cerium-oxide-nanoparticle-decorated zinc oxide with enhanced photocatalytic degradation of methyl orange. Appl Sci 10(5):1697

Rostami M (2017) Construction of La-doped TiO_2@La-doped ZnO–B-doped reduced graphene oxide ternary nanocomposites for improved visible light photocatalytic activity. RSC Adv 7:43424. https://doi.org/10.1039/C7RA06767D

Samadi M, Zirak M, Naseri A, Khorashadizade E, Moshfegh AZ (2016) Recent progress on doped ZnO nanostructures for visible light photocatalysis. Thin Solid Films 605:2–19. https://doi.org/10.1016/j.tsf.2015.12.064

Sannakashappanavar BS, Byrareddy CR, Pattanashetti NA, Singh K, Yadav AB (2019) Growth of ZnO nanorods on different seed layer thickness using the hydrothermal method for UV detection. J Nanoelectron Optoelectron 14:964–971. https://doi.org/10.1166/jno.2019.2599

Shabannia R, Naderi N (2019) High UV-to-visible rejection ratio and low cost UV photodetector based on Co-doped ZnO nanorods grown on polyethylene terephthalate substrate. J Nanoelectron Optoelectron 14:1368–1373. https://doi.org/10.1166/jno.2019.2549

Shakir M, Faraz M, Sherwani MA, Al-Resayes SI (2016) Photocatalytic degradation of the paracetamol drug using lanthanum doped ZnO nanoparticles and their in-vitro cytotoxicity assay. J Lumin 176:159–167. https://doi.org/10.1016/j.jlumin.2016.03.027

Sin JC, Lam SM (2016) Hydrothermal synthesis of europium-doped flower-like ZnO hierarchical structures with enhanced sunlight photocatalytic degradation of phenol. Mater Lett 182:223–226. https://doi.org/10.1016/j.matlet.2016.06.126

Singh K, Mehta SK (2016) Luminescent ZnO quantum dots as an efficient sensor for free chlorine detection in water. Analyst 141:2487–2492. https://doi.org/10.1039/C5AN02599K

Siriwong C, Wetchakun N, Inceesungvorn B, Channei D, Samerjai T, Phanichphant S (2012) Doped-metal oxide nanoparticles for use as photocatalysts. Prog Cryst Growth Charact Mater 58:145–163. https://doi.org/10.1016/j.pcrysgrow.2012.02.004

Thi VHT, Lee BK (2017) Effective photocatalytic degradation of paracetamol using La-doped ZnO photocatalyst under visible light irradiation. Mater Res Bull 96:171–182. https://doi.org/10.1016/j.materresbull.2017.04.028

Toal SJ, Trogler WC (2006) Polymer sensors for nitroaromatic explosives detection. J Mater Chem 16(28):2871

Trandafilovic LV, Jovanovic DJ, Zhang X, Ptasinska S, Dramicanin MD (2017) Enhanced photocatalytic degradation of methylene blue and methyl orange by ZnO: Eu nanoparticles. Appl Catal B Environ 203:740–752. https://doi.org/10.1016/j.apcatb.2016.10.063

Umar A (2017) Encyclopedia of semiconductor nanotechnology. American Scientific Publishers, New York

Umar A, Hahn YB (2010) Metal oxide nanostructures and their applications ZnO nanostructures and their nanodevices applications, vol 5. American Scientific Publishers (ASP), New York

Umar A, Chauhan MS, Chauhan S, Kumar R, Kumar G, Al-Sayari SA, Hwang HW, Al-Hajry A (2011) Large-scale synthesis of ZnO balls made of fluffy thin nanosheets by simple solution process: structural, optical and photocatalytic properties. J Colloid Interface Sci 363:521–528. https://doi.org/10.1016/j.jcis.2011.07.058

Umar A, Akhtar MS, Almas T, Ibrahim AA, Al-Assiri MS, Masuda Y, Rahman QI, Baskoutas S (2019) Direct growth of flower-shaped ZnO nanostructures on FTO substrate for dye-sensitized solar cells. Crystals 9(8):405. https://doi.org/10.3390/cryst9080405

Umar A, Ibrahim AA, Kumar R, Almas T, Sandal P, Al-Assiri MS, Mahnashi MH, Baskoutas S (2020) Fern shaped La_2O_3 nanostructures as potential scaffold for efficient hydroquinone chemical sensing application. Ceram Int 46(4):5141–5148. https://doi.org/10.1016/j.ceramint.2019.10.258

Wang ZL (2004) Zinc oxide nanostructures: growth, properties and applications. J Phys Condens Matter 16:829. https://doi.org/10.1088/0953-8984/16/25/R01

Wang ZL, Song J (2006) Piezoelectric nanogenerators based on zinc oxide nanowire arrays. Science 312:242. https://doi.org/10.1126/science.1124005

Wang ZH, Yang CC, Yu HC, Peng YM, Su YK (2018) Electron emission enhanced properties of gold nanoparticle-decorated ZnO nanosheets grown at room temperature. Sci Adv Mater 10:1675–1679. https://doi.org/10.1166/sam.2018.3396

Xiong G, Pal U, Serrano JG, Ueer KB, Williams RT (2006) Photoluminescence and FTIR study of ZnO nanoparticles: the impurity and defect perspective. Phys Status Solid (c) 3(10):3577–3581. https://doi.org/10.1002/pssc.200672164

Yang J, Yi W, Zhang L, Li T, Chao Z, Fan J (2018) Facile fabrication of ZnO nanomaterials and their photocatalytic activity study. Sci Adv Mater 10:1721–1728. https://doi.org/10.1166/sam.2018.3397

Yayapao O, Thongtem S, Phuruangrat A, Thongtem T (2013) Sonochemical synthesis, photocatalysis and photonic properties of 3% Ce-doped ZnO nanoneedles. Ceram Int 39:S563–S568. https://doi.org/10.1016/j.ceramint.2012.10.136

Ziabari SAM, Rozati SM, Najafi N (2019) Transparent conductive oxide thermoelectric (TCO-TE) generators: fabrication and comparing of ZnO, SnO_2, fluorine doped tin oxide and fluorine doped zinc oxide materials as TCO TE generators. J Nanoelectron Optoelectron 14:1331–1338. https://doi.org/10.1166/jno.2019.2631

Zheng Y, Chen C, Zhan Y, Li X, Zheng Q, Wei K, Zhu J, Zhu Y (2007) Luminescence and photocatalytic activity of ZnO nanocrystals: correlation between structure and property. Inorg Chem 46:6675–6682. https://doi.org/10.1021/ic062394m

Publisher's Note Springer Nature remains neutral with regard to jurisdictional claims in published maps and institutional affiliations.